Nanostructured ion beam-modified Ge films for high capacity Li ion battery anodes

N. G. Rudawski, B. L. Darby, B. R. Yates, K. S. Jones, R. G. Elliman et al.

Related Articles

Tin doped indium oxide core—TiO2 shell nanowires on stainless steel mesh for flexible photoelectrochemical cells
Appl. Phys. Lett. 100, 084104 (2012)

Synthesis and characterization of Nd4+xFe72Co5Ga2B17−x nanocomposite ribbons
J. Appl. Phys. 111, 07A713 (2012)

Magnetic hardening of Ce2Fe14B
J. Appl. Phys. 111, 07A718 (2012)

Thermal properties of the hybrid graphene-metal nano-micro-composites: Applications in thermal interface materials
Appl. Phys. Lett. 100, 073113 (2012)

Fabrication of single-walled carbon nanohorns containing iodine and cesium
J. Appl. Phys. 111, 044302 (2012)

Additional information on Appl. Phys. Lett.

Nanostructured ion beam-modified Ge films for high capacity Li ion battery anodes

N. G. Rudawski,[1,a)] B. L. Darby,[1] B. R. Yates,[1] K. S. Jones,[1] R. G. Elliman,[2] and A. A. Volinsky[3]

[1]*Department of Materials Science and Engineering, University of Florida, Gainesville, Florida 32611-6400, USA*
[2]*Department of Electronic Materials Engineering, Research School of Physics and Engineering, Australian National University, Canberra, Australian Capital Territory 0200, Australia*
[3]*Department of Mechanical Engineering, University of South Florida, Tampa Florida 33620, USA*

Nanostructured ion beam-modified Ge electrodes fabricated directly on Ni current collector substrates were found to exhibit excellent specific capacities during electrochemical cycling in half-cell configuration with Li metal for a wide range of cycling rates. Structural characterization revealed that the nanostructured electrodes lose porosity during cycling but maintain excellent electrical contact with the metallic current collector substrate. These results suggest that nanostructured Ge electrodes have great promise for use as high performance Li ion battery anodes. © 2012 American Institute of Physics. [http://dx.doi.org/10.1063/1.3689781]

Developing alternatives to current commercially available Li ion battery (LIB) electrode materials remains of great importance.[1] In particular, there is interest in Ge as an anode material due to very high specific capacity[2] (1623 mAh/g) and Li^+ diffusivity.[3] However, Ge experiences large volumetric changes of ∼400% during lithiation (charging) and delithiation (discharging). In nonporous thin film electrodes, this ultimately leads to intra-material fracture[4] and/or delamination at the electrode/current collector interface,[5] resulting in the loss of electrical contact and a concomitant decline in specific capacity with electrochemical cycling. Different electrode structures have been advanced to address this issue, including nanoscale films,[6] nanowires (NWs),[7,8] nanoparticle composites,[9,10] and mesoporous films.[11,12] In each case, the design principles are essentially the same: reducing the feature size(s) of the electrodes towards the nanoscale[13] to facilitate stress relaxation during cycling without decrepitation[4] and increasing specific surface area to facilitate charge transfer.

It is also interesting to consider the use of ion beam modification to create Ge anodes with nanoscale features. Specifically, recent work has revealed that ion-irradiation of Ge at very high doses results in a complete structural decomposition from nonporous material into a porous nanoscale interdigitated network of strands,[14–17] known as "nanostructured" Ge. When used as a LIB anode, the nanoscale nature of this microstructure may facilitate stress relaxation during cycling without material decrepitation, similar to other nanoscale forms of Ge. Here, the fabrication and performance of nanostructured Ge as a rechargeable LIB electrode is reported.

For this work, Ge electrodes were fabricated by first depositing Ge films 200–240-nm-thick at a rate of 0.5 nm/s onto 0.001″-thick Ni foil substrates using room-temperature electron beam evaporation. A high-resolution cross-sectional transmission electron microscopy (HR-XTEM) image of a typical "as-deposited" electrode is presented in Fig. 1(a) and indicates a continuous nonporous film. The as-deposited electrodes are also amorphous as indicated by the inset selected area electron diffraction (SAED) pattern. A portion of the as-deposited electrodes was Ge^+-implanted at room temperature at an energy of 260 keV to a dose of 1.0×10^{16} cm^{-2} in order to produce electrodes with nanostructured morphology as shown in Fig. 1(b). A porous nanoscale interdigitated network of strands characteristic of this morphology[14–17] is clearly evident and the electrode remains amorphous.

Cells for electrochemical testing were prepared in sealed pouches in an Ar atmosphere (H$_2$O concentration < 0.9 ppm) using single-ply polypropylene separators and 1.0 M LiPF$_6$ in 1:1 (by volume) ethylene carbonate:dimethyl carbonate (DMC) liquid electrolyte with the Ge film on the Ni foil as one electrode and Li metal foil as the other electrode (half-cell configuration). The electrochemical properties of each film were evaluated with galvanostatic (constant current) cycling described in detail elsewhere.[7] The charge/discharge currents needed to generate the specified cycling rates for each sample were calculated by estimating the Ge mass of each sample using the reported density[18] of evaporated Ge (4.82 g/cm^3), the surface area of the Ni foil, and the thickness
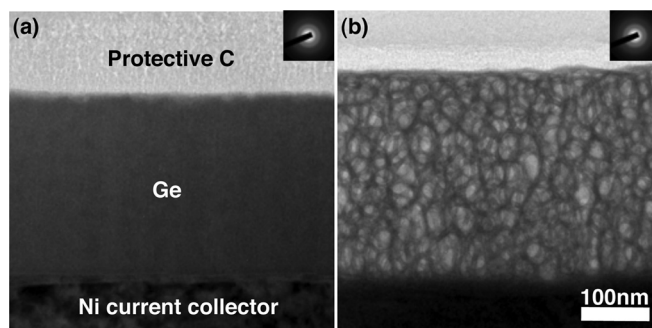

FIG. 1. HR-XTEM images (inset SAED patterns) of virgin Ge electrodes: (a) as-deposited and (b) nanostructured created via ion beam modification.

a)Author to whom correspondence should be addressed. Electronic mail: ngr@ufl.edu.

of the as-deposited films. The estimated experimental error in all mass calculations was ±5%, which result in a corresponding experimental error of the same magnitude for all reported specific capacities. Additionally, loss of Ge mass as a result of ion-irradiation to form the nanostructured morphology is expected to be negligible (<1%) as per simulations[19] and prior work;[16] the additional Ge mass resulting from ion-irradiation is also negligible (<0.001%). The morphological and structural evolution of the electrodes was evaluated with HR-XTEM and top-down/cross-sectional scanning electron microscopy (SEM); focused ion beam (FIB) milling was used to prepare HR-XTEM and cross-sectional SEM samples. Prior to FIB processing, samples were coated with C and Pt protective layers to prevent surface damage. Prior to analyzing cycled electrodes, the cells were reintroduced into the Ar environment used for fabrication and the electrodes given a 1 min wash with DMC to remove remnant electrolyte.[20] Care was taken to minimize exposure of cycled electrodes to air prior to HR-XTEM or SEM analysis.

Fig. 2(a) shows the specific capacity versus cycle behavior for a nanostructured Ge electrode cycled at a C/7.2 rate (7.2 h per charge or discharge) for 25 cycles; the corresponding behavior for the case of an as-deposited Ge film is provided for comparison. For the first cycle, the nanostructured electrode exhibited a specific charge (discharge) capacity of 1279 (1259) mAh/g with a calculated coulombic efficiency (CE) of ~98.4%. After 25 cycles, the charge (discharge) capacity was ~1352 (~1260) mAh/g indicating virtually no capacity fade. In contrast, the specific capacity of the as-deposited film faded rapidly to ~200 mAh/g after 25 cycles. Additionally, another nanostructured Ge electrode cycled at a C/7.2 cycling rate for 100 cycles showed a stable charge (discharge) capacity ~1342 (~1276) mAh/g with virtually no capacity fade (not presented). It should be noted that partial inadvertent charging occurred prior to cycling of the

nanostructured electrode used to generate the data in Fig. 2. This explains why the CE during the first cycle was much higher than expected, as Ge electrodes[6,7] are known to form a solid-electrolyte interphase layer during the first cycle.[21] Another nanostructured Ge electrode was used to evaluate the effect of sequentially changing the cycling rate on the specific capacity as shown in Fig. 2(b). Even as the cycling rate increased to C/0.9, the specific capacities were still greater than 1000 mAh/g. Following cycling at a C/0.9 rate, the rate was decreased to C/7.2, and virtually all of the capacity observed initially during cycling at a C/7.2 rate was recovered.

Voltage profiles for cycles 2 and 20 of the nanostructured Ge electrode presented in Fig. 2(a) are shown in Fig. 2(c). The profiles are similar to those reported in the literature for other Ge electrodes, mostly notably the distinct plateau at ~0.5 V during discharge.[6,9,11,12,22] Additionally, a plot of differential capacity versus voltage (relative to Li/Li+) is presented in Fig. 2(d) for cycles 2 and 20 of the nanostructured Ge electrode presented in Fig. 2(a). During cycle 2, distinct peaks during charging were evident at ~380 and ~140 mV, while distinct peaks at ~475 and ~510 mV were observed during the subsequent discharge. During the twentieth charge cycle, there was a slight shift in the peak observed at ~140 mV during the second charge cycle to ~170 mV during the twentieth charge cycle; small shifts such as this are consistent with prior results.[6] No new/ removed peaks or shifts in peak positions were evident in the twentieth discharge cycle as compared to the second charge cycle. The differential capacity data is reasonably consistent with the reported lithiation/delithiation behavior of Ge.[6,9,11,12,22] Additionally, SAED was also performed on the nanostructured Ge electrodes and indicated that the material remains amorphous after both the first charge and subsequent discharge cycle (not presented), consistent with some prior reports[7,8] of crystallographic evolution during cycling.
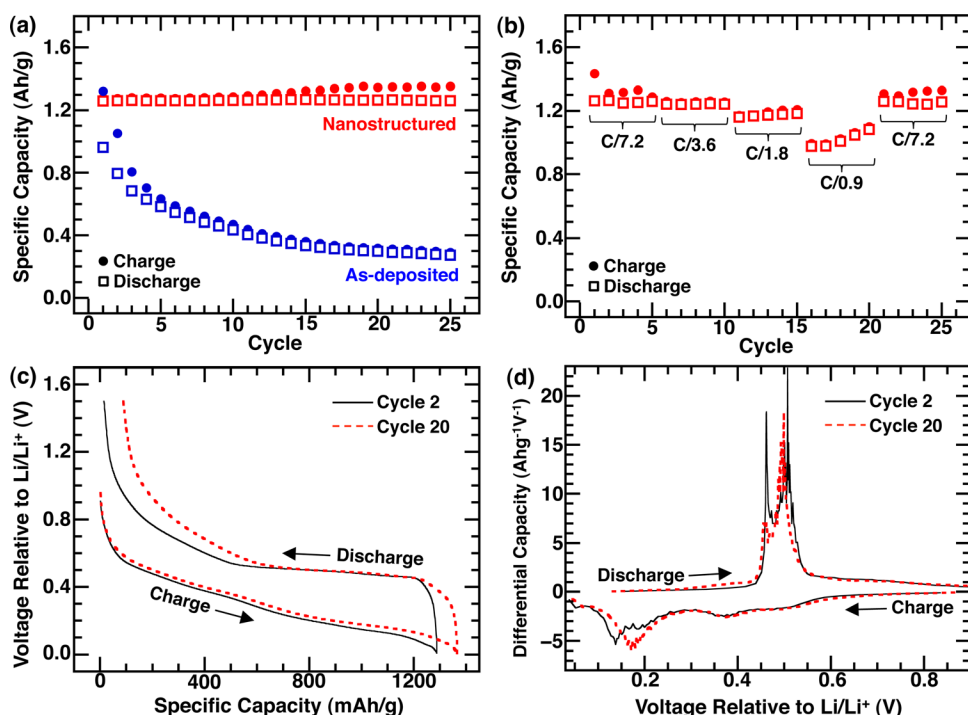

FIG. 2. (Color online) (a) Specific capacity versus cycle number data for a nanostructured Ge electrode cycled at a C/7.2 rate for 25 cycles; the data of an as-deposited Ge electrode cycled at the same rate is provided for comparison. (b) Specific capacity versus cycle number data for a nanostructured Ge electrode cycled sequentially at C/7.2, C/3.6, C/1.8, C/0.9, and C/7.2 rates (5 cycles each, 25 cycles total). (c) Voltage profiles for cycles 2 and 20 of the nanostructured Ge electrode in (a). (d) Differential capacity profiles for cycles 2 and 20 of the nanostructured Ge electrode in (a).
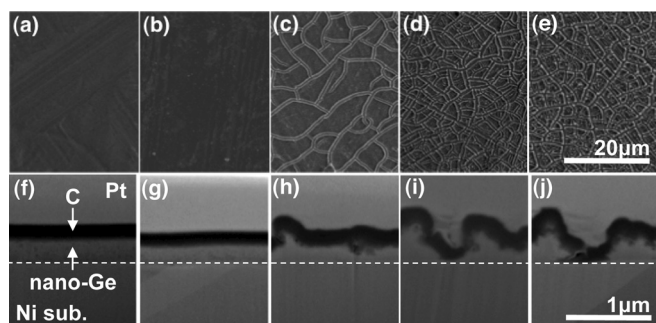
FIG. 3. Top-down SEM images showing the morphological evolution of nanostructured Ge electrodes during electrochemical cycling at a C/7.2 rate: (a) 0, (b) 1, (c) 8, (d) 16, and (e) 25 cycles. Cross-sectional SEM images taken at 52° incident angle showing the morphological evolution of nanostructured Ge electrodes during electrochemical cycling at a C/7.2 rate: (f) 0, (g) 1, (h) 8, (i) 16, and (j) 25 cycles. The protective Pt/C layers, nanostructured Ge film ("nano-Ge"), and Ni substrate are indicated.

FIG. 4. HR-XTEM images (inset SAED patterns) showing the morphological evolution of nanostructured Ge electrodes with electrochemical cycling at a C/7.2 rate: (a) an untested electrode and (b) an electrode after 25 cycles.

Figs. 3(a)–3(e) present top-down SEM images of the structural evolution of a nanostructured Ge electrode with electrochemical cycling at a C/7.2 rate. Compared to the virgin electrode, shown in Fig. 3(a), the surface of the electrode was unchanged after 1 cycle, as shown in Fig. 3(b). However, significant through-thickness cracking was evident after 8 cycles as shown in Fig. 3(c). The degree of cracking increased further after 16 cycles as presented in Fig. 3(d), but no appreciable change in the cracking pattern was observed after 25 cycles as presented in Fig. 3(e). The evolution of the nanostructured Ge electrode with cycling was also observed in cross-section using a combination of FIB milling and SEM at an incident angle of 52°, as shown in Figs. 3(f)–3(j). As compared to the virgin electrode shown in Fig. 3(f), the electrode remained flat and unperturbed after 1 cycle as indicated in Fig. 3(g). However, after 8 cycles, roughening of the electrode near crack edges was evident as presented in Fig. 3(h). The roughness increased further after 16 cycles as shown in Fig. 3(i) and remained basically unchanged after 25 cycles as shown in Fig. 3(j). Additionally, the structural evolution of the nanostructured Ge electrodes was investigated using HR-XTEM as shown in Fig. 4. The initial porous nanoscale interdigitated network of strands present in the untested nanostructured electrode in Fig. 4(a) was no longer evident after 25 cycles at a C/7.2 cycling rate, shown in Fig. 4(b); in fact, it appears the electrode lost detectable porosity.

The dramatic structural evolution of the nanostructured Ge electrodes with electrochemical cycling is very intriguing considering that other nanoscale Ge electrodes undergo much subtler morphological changes with cycling. However, in the case of the nanostructured Ge electrodes, the initial nanoscale interdigitated network of strands was lost after cycling, resulting in loss of porosity of the electrode. In fact, analogous behavior has been observed in the case of some nanoparticle-based electrodes where the nanoparticles tend to agglomerate together with cycling.[23–25] This process has been referred to as "electrochemical sintering," and although it is still poorly understood, it is reasonable to believe that the nanostructured morphology is inherently unstable as it has a very high surface area to volume ratio. Thus, it may be that the system is placed in an activated state during electro-
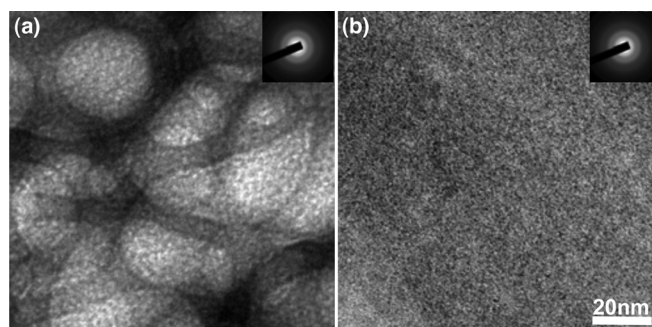
chemical cycling such that the transformation to a nonporous film may occur. The loss of porosity with electrochemical cycling can also explain the formation of through-thickness cracks, since it is known that nonporous film electrodes of sufficient thickness will exhibit cracking with electrochemical cycling.[26]

However, the performance of the nanostructured electrodes, even after losing the porous nanostructured morphology, is vastly superior to the nonporous as-deposited electrodes. The reason for the large difference in performance may be reasonably attributed to nearly all of the mass of the nanostructured electrode remaining in excellent electrical contact with the current collector (even after loss of the nanostructured morphology). This implies that loss of electrical contact due to intra-material fracture[4] and delamination[5] at the electrode/current collector interface are avoided. Of course, intra-material fracture is not totally avoided, since the through-thickness cracking observed results from intra-material fracture. However, through-thickness cracking does not result in material losing electrical contact and therefore does not degrade performance. Additionally, the extensive through-thickness cracking presumably allows the nanostructured electrode to retain substantial surface area even after losing the nanostructured morphology, which should facilitate easier charge transfer.

The avoidance of the loss of electrical contact due to intra-material fracture (as opposed to through-thickness cracking) is due primarily to morphological considerations of the electrode material. In the case of NW and nanoparticle electrodes, the feature sizes of the individual constituents are small enough such that the large stresses associated with electrochemical cycling can be accommodated without intra-nanowire or -nanoparticle fracture. This also explains why the nanostructured morphology would allow for accommodation of the large stresses associated with cycling, since the feature sizes of the microstructure are comparable to NWs and nanoparticles. However, the nanostructured morphology was lost with cycling, and yet loss of electrical contact due to intra-material fracture was avoided. This can be partly explained by through-thickness cracking of the electrode into individual islands during cycling since significant stress relaxation is expected when the islands have a sufficiently large height to width ratio.[27] Therefore, the initial nanostructured morphology may facilitate through-thickness crack evolution during cycling into an electrode geometry that can effectively accommodate stress without loss of electrical

contact due to intra-material fracture as the electrode loses porosity with cycling.

The other main consideration, integrity of the contact between the electrode material and current collector, is related primarily to the adhesion strength between the two[26] and to a lesser extent geometric considerations.[27] In particular, ion-irradiation to produce the nanostructured electrodes likely resulted in ion beam mixing at the electrode/current collector interface. This process is known to enhance the adhesion strength between a film and substrate by up to two orders of magnitude,[28,29] which may have contributed to the lack of material delamination observed for the nanostructured electrodes. In fact, after electrochemical cycling for 25 cycles, for the as-deposited (not ion-irradiated) Ge electrodes, virtually the entire Ge film delaminated from the Ni foil substrate during DMC washing, whereas no delamination was observed for the nanostructured Ge electrodes. Furthermore, "scotch tape" adhesion tests[30] performed on virgin nanostructured electrodes produced no delamination while as-deposited electrodes delaminated easily; this provides additional evidence for improved adhesion from ion beam mixing. Of course, the individual roles of the nanostructured morphology, through-thickness crack evolution, and ion beam mixing on electrode performance are still unclear, and future experiments will attempt to address this.

In conclusion, nanostructured Ge electrodes created via ion beam-modification of as-deposited Ge films were shown to have some of the highest specific capacities reported for Ge electrodes. The performance may be associated with the ability of nanostructured Ge to accommodate the stresses associated with cycling via through-thickness crack evolution due to electrochemical sintering and/or improved adhesion from ion beam mixing.

[1] J. M. Tarascon and M. Armand, Nature **414**, 359 (2001).
[2] J. Sangster and A. Pelton, J. Phase Equilb. **18**, 289 (1997).
[3] C. S. Fuller and J. C. Severiens, Phys. Rev. **96**, 21 (1954).
[4] R. Huggins and W. Nix, Ionics **6**, 57 (2000).
[5] F. Q. Yang, J. Power Sources **196**, 465 (2011).
[6] J. Graetz, C. C. Ahn, R. Yazami, and B. Fultz, J. Electrochem. Soc. **151**, A698 (2004).
[7] C. K. Chan, X. F. Zhang, and Y. Cui, Nano Lett. **8**, 307 (2008).
[8] M. H. Seo, M. Park, K. T. Lee, K. Kim, J. Kim, and J. Cho, Energy Environ. Sci. **4**, 425 (2011).
[9] H. Lee, H. Kim, S. G. Doo, and J. Cho, J. Electrochem. Soc. **154**, A343 (2007).
[10] M.-H. Park, K. Kim, J. Kim, and J. Cho, Adv. Mater. **22**, 415 (2010).
[11] B. Laforge, L. Levan-Jodin, R. Salot, and A. Billard, J. Electrochem. Soc. **155**, A181 (2008).
[12] L. C. Yang, Q. S. Gao, L. Li, Y. Tang, and Y. P. Wu, Electrochem. Commun. **12**, 418 (2010).
[13] P. G. Bruce, B. Scrosati, and J. M. Tarascon, Angew. Chem.-Int. Ed. **47**, 2930 (2008).
[14] B. L. Darby, B. R. Yates, N. G. Rudawski, K. S. Jones, A. Kontos, and R. G. Elliman, Thin Solid Films **519**, 5962 (2011).
[15] R. J. Kaiser, S. Koffel, P. Pichler, A. J. Bauer, B. Amon, A. Claverie, G. Benassayag, P. Scheiblin, L. Frey, and H. Ryssel, Thin Solid Films **518**, 2323 (2010).
[16] L. Romano, G. Impellizzeri, M. V. Tomasello, F. Giannazzo, C. Spinella, and M. G. Grimaldi, J. Appl. Phys. **107**, 084314 (2010).
[17] B. Stritzker, R. G. Elliman, and J. Zou, Nucl. Instrum. Methods Phys. Res. B **175**, 193 (2001).
[18] G. Peto, Z. F. Horvath, O. Gereben, L. Pusztai, F. Hajdu, and E. Svab, Phys. Rev. B **50**, 539 (1994).
[19] J. F. Ziegler, Nucl. Instrum. Methods Phys. Res. B **219**, 1027 (2004).
[20] G. M. Veith and N. J. Dudney, J. Electrochem. Soc. **158**, A658 (2011).
[21] E. Peled, J. Electrochem. Soc. **126**, 2047 (1979).
[22] L. Baggetto and P. H. L. Notten, J. Electrochem. Soc. **156**, A169 (2009).
[23] H. Li, X. Huang, L. Chen, Z. Wu, and Y. Liang, Electrochem. Solid-State Lett. **2**, 547 (1999).
[24] H. Li, X. Huang, L. Chen, G. Zhou, Z. Zhang, D. Yu, Y. Jun Mo, and N. Pei, Solid State Ionics **135**, 181 (2000).
[25] H. Li, L. Shi, W. Lu, X. Huang, and L. Chen, J. Electrochem. Soc. **148**, A915 (2001).
[26] J. C. Li, A. K. Dozier, Y. C. Li, F. Q. Yang, and Y. T. Cheng, J. Electrochem. Soc. **158**, A689 (2011).
[27] A. G. Evans and J. W. Hutchinson, Int. J. Solids Struct. **20**, 455 (1984).
[28] J. E. E. Baglin, Nucl. Instrum. Methods Phys. Res. B **65**, 119 (1992).
[29] J. E. Pawel, C. J. McHargue, L. J. Romana, and J. J. Wert, Surf. Coat. Technol. **51**, 129 (1992).
[30] A. A. Volinsky, N. R. Moody, and W. W. Gerberich, Acta Mater. **50**, 441 (2002).